Ultrasound-Based Characterization of Prostate Cancer: An *in vivo* Clinical Feasibility Study

Farhad Imani[1], Purang Abolmaesumi[2], Eli Gibson[3], Amir Khojaste Galesh-Khale[1], Mena Gaed[3], Madeleine Moussa[4], Jose A. Gomez[4], Cesare Romagnoli[3], D. Robert Siemens[5], Michael Leviridge[5], Silvia Chang[6], Aaron Fenster[3], Aaron D. Ward[3], and Parvin Mousavi[1]

[1] Queen's University, Kingston, Ontario, Canada
[2] The University of British Columbia, Vancouver, British Columbia, Canada
[3] University of Western Ontario, London, Ontario, Canada
[4] London Health Science Centre, London, Ontario, Canada
[5] Kingston General Hospital, Kingston, Ontario, Canada
[6] Vancouver General Hospital, Vancouver, British Columbia, Canada

Abstract. This paper presents the results of an *in vivo* clinical study to accurately characterize prostate cancer using new features of ultrasound RF time series. *Methods:* The mean central frequency and wavelet features of ultrasound RF time series from seven patients are used along with an elaborate framework of ultrasound to histology registration to identify and verify cancer in prostate tissue regions as small as 1.7 mm $\times$ 1.7 mm. *Results:* In a leave-one-patient-out cross-validation strategy, an average classification accuracy of 76% and the area under ROC curve of 0.83 are achieved using two proposed RF time series features. The results statistically significantly outperform those achieved by previously reported features in the literature. The proposed features show the clinical relevance of RF time series for *in vivo* characterization of cancer.

Keywords: RF time series, tissue characterization, prostate cancer.

1 Introduction

Prostate cancer (PCa) is the most commonly diagnosed malignancy, and the second leading cancer-related cause of death in North American men. If diagnosed, PCa can be managed with a long-term disease free survival rate above 90%; even if determined later, radiotherapy or ablation interventions can be used to increase the life expectancy of patients. The definitive diagnosis of PCa is core needle biopsy, under ultrasound guidance [1]. The biopsy procedure entails systematic sampling of the prostate from predefined anatomical locations, followed by histopathological examination of the sampled tissue. Often, this procedure is performed in a blind manner, since conventional ultrasound imaging is rarely capable of distinguishing cancerous and normal tissue with high specificity and sensitivity. Several techniques have been proposed to enable targeted biopsy by extracting tissue-specific information from the ultrasound signal, and using this information to improve the detection rate of cancer [2].

K. Mori et al. (Eds.): MICCAI 2013, Part II, LNCS 8150, pp. 279–286, 2013.

Computer-aided methods that use ultrasound data for PCa detection utilize features extracted from Radio Frequency (RF) and B-mode ultrasound images. Texture features extracted from B-mode images have been previously applied to detect PCa [3]. The major limitations of B-mode images are the existence of speckle and loss of information due to post-processing of the ultrasound signal [4]. Features obtained from a single RF frame [5], and their combination with image-based texture features have also been utilized to classify PCa [6]. However, in practice, these features are sensitive to diffraction effects and local spectral noise. In the past decade, elastography has emerged as another approach to augment conventional ultrasound imaging for detection of PCa. In this method, various mechanical properties of the tissue are identified by generating tissue displacements using external mechanical stimulus or high energy acoustic radiation [7,8]. This approach requires external excitation of the tissue, or modification of the ultrasound hardware for applying relatively strong acoustic radiation forces.

Recently, a sequence of ultrasound RF frames captured in time, from a stationary tissue location (hereafter referred to as *RF time series*) has been used for tissue characterization [9,10]. This method has been effectively applied to classify cancerous and normal tissue regions in 35 *ex vivo* human prostate specimens [9] and six *in vivo* cancer subjects [10]. It has also been shown that this method outperforms tissue characterization approaches that use features of a single RF ultrasound frame or texture information from B-mode images [9].

In this paper, we use two new features of ultrasound RF time series to characterize PCa in an *in vivo* clinical feasibility study with seven patients. We demonstrate that these two features along with an elaborate RF time series-to-histology registration framework accurately highlight cancer in tissue regions as small as 1.7 mm×1.7 mm. We show in cross-validation experiments that the features obtained from tissue regions in a group of patients can be used to characterize the cancerous regions in an unseen patient. Our approach improves the average area under the Receiver Operating Characteristic (ROC) curve compared to previously reported results in the literature [10].

2 Materials and Methods

2.1 Data Acquisition

Following institutional research ethics board approval, a cohort of seven patients who selected prostatectomy as their choice of treatment were recruited. Patients provided informed consent to participate in this study. Prior to prostatectomy, three-dimensional (3D) B-mode and RF ultrasound data were collected using a SonixTouch ultrasound scanner (Ultrasonix, Richmond, Canada) and a BPL9-5/55 side firing transducer mounted in a motorized cradle held by a clinician. During imaging, the subjects were in a supine position with knees raised. A fan of parasagittal B-mode ultrasound images with 0.12 mm axial by 0.12 mm lateral pixel size were taken at intervals of 0.5°, and reconstructed to a 3D image with 0.12 mm isotropic voxels. The 3D RF time series data consists of a fan of 2D RF time series data with 2° rotational intervals, where each 2D RF time series data

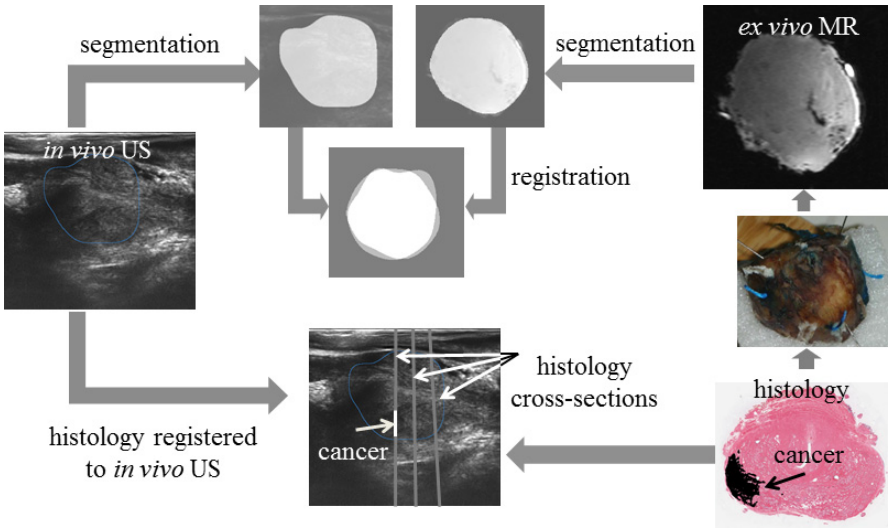

Fig. 1. The workflow for registration of *in vivo* ultrasound to histology images

comprises 128 frames taken at a frame rate of 77 frames/sec with a 0.85 mm lateral by 0.04 mm axial pixel size. Ultrasound data were taken with a frequency of 6.67 MHz, a depth of 5 cm, and constant time gain compensation.

After resection, the prostate specimens were processed following a protocol to facilitate 3D reconstruction of whole-mount histology [11]. After fixation in 10% buffered formalin, MR- and histology-visible strand-shaped fiducial markers were applied to the specimen internally and externally following a prescribed layout [11]. *Ex vivo* MR images of the marked specimen were acquired on a Discovery MR750 scanner (GE Healthcare, Waukesha, USA) at 3T using an endorectal coil (Prostate eCoil, Medrad, Warrendale, USA) with a T1-weighted MR protocol yielding images with 0.3 mm voxel spacing. Following MR imaging, the prostatic apex was removed and the midgland was cut on a rotary slicer into three to five 4.4 mm thick tissue slices for histological processing and paraffin embedding. A 4 μm thick histology section was cut from each paraffin block, mounted on a positively charged slide, stained with hematoxylin and eosin and digitized on a ScanScope GL (Aperio Tech., Vista, USA) bright field slide scanner yielding histology images with 0.5 μm pixels. Cancerous regions with a Gleason grade of 3 and higher were contoured on the digitized histology images by a clinician and confirmed by a genitourinary pathologist. Regions of the prostate with benign prostatic hyperplasia (BPH) and atrophy were also contoured.

2.2 Image Registration and Region of Interest Selection

To classify cancerous and normal tissue, RF time series features are extracted over small regions of interest (ROIs). A set of 415 equally-sized ROIs are selected from ultrasound images of all subjects. The size of each ROI is 1.7 mm $\times$ 1.7 mm;

in other words, RF time series data from an ROI comprises a 3D signal with 44 axial, 2 lateral and 128 time samples. The ratio of the number of cancerous and normal ROIs is 1:1. To select the cancerous and normal ROIs, histology images are registered to *in vivo* ultrasound B-mode images corresponding to RF data (Fig. 1). This registration is performed in two steps: registration of *ex vivo* MR to histology and registration of *in vivo* ultrasound to *ex vivo* MR images.

Registration of ex vivo MR to histology images: Histology images are registered to *ex vivo* MR images using a fiducial-based algorithm [11]. The center points of the cross-sections of the strand-shaped fiducials on histology images are interactively identified and the parametric curves corresponding to the center lines of the strand-shaped fiducials on the *ex vivo* MR images are identified semi-automatically. The 2D-3D affine transformation from each histology image to the corresponding *ex vivo* MR image is identified by minimizing the fiducial registration error between the identified fiducial points and corresponding fiducial curves in the two modalities with target registration error of 0.7 mm.

Registration of in vivo ultrasound to ex vivo MR images: The registration steps of *in vivo* ultrasound to *ex vivo* MR images are presented in Fig. 1. The prostate boundaries in *in vivo* ultrasound and *ex vivo* MR images are segmented manually by a graduate student familiar with ultrasound and MR images, and verified by an expert clinician. The generated labeled prostate regions are then manually aligned; the prostate orientation in the *in vivo* ultrasound images can be easily discerned, while surface mounted fiducials of each specimen are used to determine the gland orientation in the *ex vivo* MR images [11]. Subsequently, an intensity-based affine registration is applied to register the aligned images.

Histology images are transformed to the coordinates of ultrasound images. Since the histology images are obtained from approximately transverse sections, whereas ultrasound is taken in the parasagittal plane, the intersection of data from these two modalities appear as approximately-parallel lines in ultrasound images. As such, cancerous regions are highlighted in ultrasound data as depicted in Fig. 2. To select the cancerous and normal ROIs, we consider the effect of possible registration error; we choose cancerous ROIs from dominant lesions with an average size of 17 mm where cancer appears in consecutive histology slices, while we leave a safe margin of more than 5 mm away from cancer, BPH and atrophy to select the normal ROIs.

2.3 Feature Extraction and Classification

To extract the RF time series features, the mean of each ultrasound RF time series is removed, and its spectrum is calculated. The result is averaged over each ROI. Subsequently, two features are computed, as described below.

Mean Central Frequency (MCF): We calculate the central frequency of the RF time series spectrum, $CF = \sum_{n=1}^{N/2} Kn.\,|[FFT(TS)](n)| / \sum_{n=1}^{N/2} |[FFT(TS)](n)|$, where N=128 is the number of time samples in each RF time series, K is a constant denoting the spacing of frequencies, and $|[FFT(TS)](n)|$ is the amplitude of the spectrum of the RF time series. The mean of these CF values in an ROI constitutes the MCF feature of that ROI.

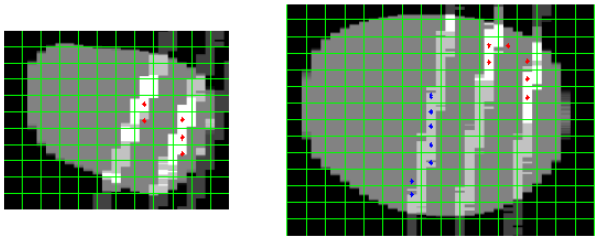

Fig. 2. Cross-sections of histology slices overlaid on segmented ultrasound images. The selected cancerous and normal ROIs are shown with red and blue stars.

Wavelet: A discrete wavelet transform of the RF time series is computed using the Daubechies-4 filter bank. The signal is decomposed into detail and approximation coefficients at each level. The average of the first approximation coefficients at level 10 over an ROI is extracted and used as the wavelet feature. In our dataset, we determined that choosing the tenth level of decomposition lead to the best tissue characterization results.

We also compute previously reported RF time series features that were used in *in vivo* characterization of PCa [10]. These include the summation of the spectrum of the RF time series at three frequency bands, and the intercept and slope of the fitted line to the spectrum in the entire frequency range. We refer to these features as those from Moradi *et al.*.

A support vector machine (SVM) is used to classify cancerous and normal ROIs[1]. A kernel function maps the training data to a higher dimension, and the data are separated into two classes by a hyperplane. The radial basis function is our kernel of choice due to its ease of initialization and classification accuracy [9]. The only parameter of this kernel that requires initialization is the inverse of variance; its optimal value resulting in highest classification accuracy is determined by a coarse followed by a fine heuristic search. In addition to the binary class labels, the probability of the tested data representing cancer is also provided by the SVM classifier.

3 Experiments and Results

We follow a leave-one-patient-out cross-validation strategy. A classifier is trained using extracted RF time series features from the ROIs of a selected group of subjects (six subjects) with known labels, and tested on the features of the ROIs of the remaining subject. The histograms of the MCF and wavelet features of the RF time series, in normal and cancerous ROIs of seven subjects, are shown in Fig. 3. The classification accuracies achieved using these two features are 87%, 53%, 78%, 62%, 68%, 88%, and 94% with an average of 76±15% as presented in Table 1. The ROC curves for these evaluations are also plotted in Fig. 4. The

[1] A Library for SVMs, `http://www.csie.ntu.edu.tw/~cjlin/libsvm/`

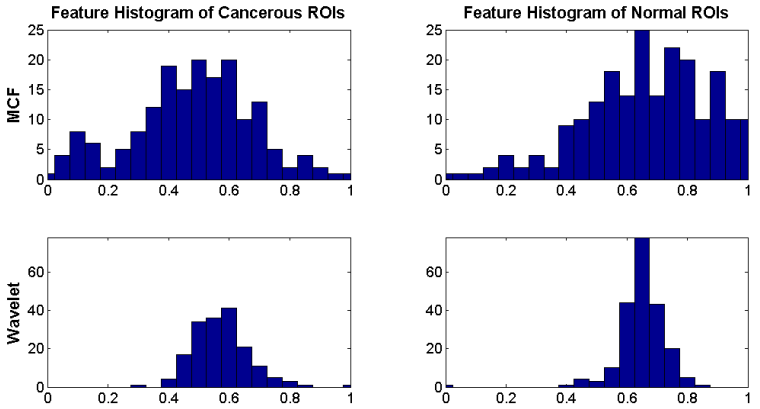

Fig. 3. Histogram of the proposed features for normal and cancerous ROIs (n=7)

Table 1. Classification accuracies for leave-one-patient-out evaluations using MCF and wavelet features and previously presented features in the literature

Subject	1	2	3	4	5	6	7	Mean
MCF	74%	55%	86%	63%	57%	74%	70%	68±11%
Wavelet	87%	63%	65%	60%	65%	79%	90%	73±12%
MCF and wavelet	87%	53%	78%	62%	68%	88%	94%	76±15%
Moradi *et al.* features	66%	33%	79%	61%	50%	68%	63%	60±15%

areas under the ROC (AROC) curves for the seven subjects are 0.96, 0.59, 0.84, 0.72, 0.71, 0.98, and 0.98, respectively with an average of 0.83.

We also apply the classifier built using MCF and wavelet features from a group of patients to classify the entire imaging planes of a left-out patient. The colormaps of the cross-sections of the histology slices overlaid on the ultrasound images are depicted in Fig. 5 for three examples. These examples are selected from the subjects with high classification outcomes. As mentioned above, these colormaps are generated through leave-one-patient-out cross-validation; the colormaps are only displayed for an ROI on the image if the cancer probability in that ROI is ≥ 0.5. The class probability estimates are provided by the SVM.

Finally, we compute the classification accuracies, and the AROC curves obtained using the features proposed by Moradi *et al.*. The means of the classification accuracies, and AROC curves are 60% and 0.64 for leave-one-patient-out evaluations. The classification results obtained by the two proposed RF time series features statistically significantly outperform those achieved using Moradi et al. features ($p = 0.02$, Mann-Whitney U-test). Since we only have limited data points to test for statistical significance, we opted for a non-parametric test.

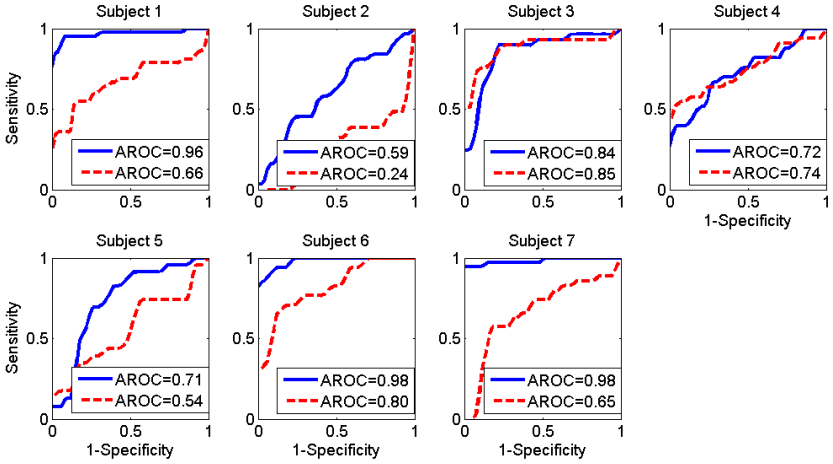

Fig. 4. ROC curves and AROC for leave-one-patient-out evaluations. The blue solid and red dashed graphs represent the ROC curves obtained using the two proposed RF time series features in this paper and those of Moradi *et al.*, respectively.

4 Discussion and Conclusion

RF time series data have been utilized previously to improve the accuracy and sensitivity of conventional ultrasound methods for tissue characterization at both high and clinical frequencies. This method has been shown to outperform tissue characterization using features of single RF ultrasound frames or texture information from B-mode images. In this paper, we present a clinical feasibility study for *in vivo* characterization of cancerous ROIs as small as 1.7 mm×1.7 mm with Gleason grade of 3 or higher using MCF and wavelet features of RF time series. A leave-one-patient-out cross-validation strategy was applied and RF time series data from seven human prostates were used. An average classification accuracy of 76% and an area under the ROC curve of 0.83 are achieved by training a classifier using MCF and wavelet features extracted from six patients, and using the classifier to predict normal and cancerous tissue of unseen patients. However, the small tumor size of subject 2, and various pathological heterogeneities of subjects 4 and 5, along with their larger registration errors compared to other cases caused lower classification accuracies for these three subjects. We also generated colormaps of the cancer probability by training a classifier with MCF and wavelet features of a group of patients and using it to characterize tissue not only in the ROIs but also in the entire imaging plane of unseen patients.

Although care was taken in this study to select ROIs with consideration of the effect of registration error, our ongoing work includes the use of deformable registration between the *in vivo* ultrasound and *ex vivo* MR images to further mitigate this issue. MCF and wavelet features of ultrasound RF time series outperform significantly Moradi *et al.* features using the data acquisition protocol in this study. For clinical translation of the proposed features, large scale

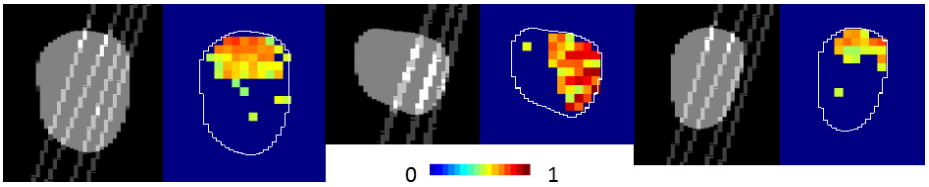

Fig. 5. Cross-sections of histology slices in the parasagittal planes overlaid on segmented *in vivo* ultrasound images for three examples (left images); corresponding cancer probability colormaps generated using the two proposed RF time series features, through leave-one-patient-out evaluation, and extended to entire imaging planes (right images); top is posterior, bottom is anterior, right is apex, and left is base of the gland

studies should be performed to determine the best combination of RF time series features along with their consistency for *in vivo* characterization of cancer.

Acknowledgments. This work was supported in part by the Natural Sciences and Engineering Research Council of Canada (NSERC), the Canadian Institutes of Health Research (CIHR), Queen's University, and Ontario Early Researcher Award.

References

1. Hodge, A.C., Fenster, A., Downey, D.B., Ladak, H.M.: Prostate boundary segmentation from ultrasound images using 2D active shape models: Optimisation and extension to 3D. Comput. Methods Programs Biomed. 84, 99–113 (2006)
2. Inahara, M., Suzuki, H., Nakamachi, H., et al.: Clinical evaluation of transrectal power doppler imaging in the detection of PCa. Int. Urol. Neph. 36, 175–180 (2004)
3. Han, S.M., Lee, H.J., Choi, J.U.: Computer-aided PCa detection using texture features and clinical features in ultrasound image. Digit. Imaging 21, 121–133 (2008)
4. Tsui, P.H., Chang, C.C.: Imaging local scatterer concentrations by the Nakagami statistical model. Ultrasound Med. Biol. 33, 608–619 (2007)
5. Feleppa, E., Porter, C., Ketterling, J., et al.: Recent developments in tissue-type imaging for planning and monitoring treatment of PCa. US Img. 26, 163–172 (2004)
6. Schmitz, G., Ermert, H., Senge, T.: Tissue-characterization of the prostate using RF ultrasonic signals. IEEE Trans. Ultrason. Ferr. Freq. Control 46, 126–138 (1999)
7. Salcudean, S.E., French, D., Bachmann, S., Zahiri-Azar, R., Wen, X., Morris, W.J.: Viscoelasticity modeling of the prostate region using vibro-elastography. In: Larsen, R., Nielsen, M., Sporring, J. (eds.) MICCAI 2006. LNCS, vol. 4190, pp. 389–396. Springer, Heidelberg (2006)
8. Zhai, L., Madden, J., Foo, W.C., et al.: Acoustic radiation force impulse imaging of human prostates ex vivo. Ultrasound Med. Biol. 36, 576–588 (2010)
9. Moradi, M., Abolmaesumi, P., Siemens, R., et al.: Augmenting detection of PCa in transrectal US images using SVM and RF TS. IEEE TBME 56, 2214–2224 (2009)
10. Moradi, M., Mahdavi, S., Nir, G., et al.: US RF time series for tissue typing: first in-vivo clinical results. In: SPIE (2013)
11. Gibson, E., Crukley, C., Gaed, M., et al.: Registration of prostate histology images to ex vivo MR images via strand-shaped fiducials. JMRI 36, 1402–1412 (2012)